Biochem. J. (2014) **464**, 449–459 (Printed in Great Britain) doi:10.1042/BJ20140679



# The disease-associated mutation of the mitochondrial thiol oxidase Erv1 impairs cofactor binding during its catalytic reaction

Efrain Ceh-Pavia*, Swee Kim Ang*, Michael P. Spiller* and Hui Lu*[1]

*Faculty of Life Sciences, Manchester Institute of Biotechnology, University of Manchester, 131 Princess Street, Manchester M1 7DN, U.K.

Erv1 (essential for respiration and viability 1) is an FAD-dependent thiol oxidase of the Erv/ALR (augmenter of liver regeneration) sub-family. It is an essential component of the mitochondrial import and assembly (MIA) pathway, playing an important role in the oxidative folding of the mitochondrial intermembrane space (IMS) proteins and linking the MIA pathway to the mitochondrial respiratory chain via cytochrome *c* (cyt *c*). The importance of the Erv/ALR enzymes was also demonstrated in a recent study where a single mutation in the human ALR (R194H) leads to autosomal recessive myopathy [Di Fonzo, Ronchi, Lodi, Fassone, Tigano, Lamperti, Corti, Bordoni, Fortunato, Nizzardo et al. (2009) Am. J. Hum. Genet. **84**, 594–604]. However, the molecular mechanism of the disease is still unclear. In the present study, we use yeast Erv1 as a model to provide clear evidence for a progressive functional defect in the catalytic activity of the corresponding Erv1 R182H mutant. We show that the FAD cofactor was released from Erv1 R182H during its catalytic cycle, which led to the inactivation of the enzyme. We also characterized the effects of the mutation on the folding and stability of Erv1 and tested our *in vitro* findings *in vivo* using a yeast genetic approach. The results of the present study allow us to provide a model for the functional defect in Erv1 R182H, which could potentially be extended to human ALR R194H and provides insights into the molecular basis of autosomal recessive myopathy.

Key words: autosomal recessive myopathy, enzymology, FAD-binding, mitochondrial import and assembly (MIA) pathway, thiol oxidase.

## INTRODUCTION

The majority of mitochondrial proteins are nuclear-encoded and need to be imported into mitochondria for their function. In the mitochondrial intermembrane space (IMS), the mitochondrial import and assembly (MIA) pathway plays an essential role in the biogenesis of many mitochondrial IMS proteins. The MIA pathway consists of two essential components: the disulfide carrier Mia40 and the disulfide bond generator Erv1/ALR (essential for respiration and viability 1/augmenter of liver regeneration) [1–3]. *Saccharomyces cerevisiae* Erv1 is a thiol oxidase belonging to the single domain Erv/ALR sub-family and, like all members of the family, it contains a highly conserved FAD-binding domain of approximately 100 amino acids (Figure 1). This FAD-binding domain acts as a catalytic core and contains a CXXC active-site disulfide located proximal to the iso-alloxazing ring of FAD, as well as a C-terminal $CX_{16}C$ structural disulfide [4–8]. The crystal structures of the FAD-binding domain of Erv1 portrayed it as a head-to-tail homodimer (PDB codes 4E0H and 3W4Y) where each subunit contains a four-helix bundle that harbours the FAD cofactor and an additional (H5) C-terminal single-turn helix (Figure 1c) [9]. Erv/ALR proteins also have a shuttle disulfide bond in a non-conserved range located on either the N- or the C-terminus of the FAD-binding domain. In Erv1, the shuttle disulfide ($Cys^{30}$–$Cys^{33}$) is located in the N-terminus upstream of the active-site disulfide ($Cys^{130}$–$Cys^{133}$) (Figure 1a) [7,8].

Most substrates of the MIA pathway contain cysteine residues and many have conserved twin $CX_3C$ or $CX_9C$ motifs, hence, thiol-disulfide redox regulation has been shown to play a key role in the pathway [3,10–13]. As the cysteine-reduced precursor proteins enter the IMS, Mia40 interacts with them by forming an intermolecular disulfide-linked complex [14,15]. The Mia40 redox-active CPC disulfide bond is then transferred to the substrate proteins, leaving Mia40 in a reduced state. Next, the now CPC-reduced Mia40 (rMia40) is re-oxidized by Erv1/ALR to allow for another substrate oxidation cycle. In the case of Erv1, it is the N-terminal $Cys^{30}$–$Cys^{33}$ shuttle disulfide that first accepts the electrons from rMia40 and transfers them to the $Cys^{130}$–$Cys^{133}$ active-site disulfide, from where they are then passed to Erv1-bound FAD [12,16–19]. Finally, the FAD-reduced Erv1 (Erv1-$FADH_2$) is re-oxidized by transferring the electrons to either oxidized cytochrome *c* (cyt *c*) or molecular oxygen, thereby regenerating Erv1 activity. Through the Erv1 interaction with cyt *c*, the MIA pathway is linked to the respiratory chain [20–23].

Di Fonzo et al. [24] reported the first disease directly related to ALR, the human homologue of Erv1. The authors identified a single arginine-to-histidine substitution (R194H) in the C-terminus of ALR in children with autosomal recessive myopathy. At the cellular level, the effects included a lower cysteine-rich protein content, respiratory-chain deficiency, abnormal mitochondrial morphology and increased accumulation of mitochondrial DNA (mtDNA) deletions [24]. Because this arginine residue is conserved in other ALR homologues (Figure 1b), the authors also used yeast to show that the corresponding *erv1 R182H* mutant strain displayed genetic instability of the mtDNA, altered mitochondrial morphology, a temperature-sensitive growth phenotype and reduced cyt *c* oxidase (complex IV) activity [24]. Protein characterizations of human ALR have since then shown that the R194H mutation affects the thermal stability, FAD-binding and proteolysis

Abbreviations: ALR, augmenter of liver regeneration; BA, buffer A; BAE, buffer AE; BV, bed volumes; cyt *c*, cytochrome *c*; Erv, essential for respiration and viability; Erv1-$FADH_2$, FAD-reduced Erv1; fFAD, free FAD; IMS, intermembrane space; MIA, mitochondrial import and assembly; mtDNA, mitochondrial DNA; rMia40, CPC-reduced Mia40; SEC, size-exclusion chromatography; TCEP, tris-(2-carboxyethyl)phosphine; $T_m$, melting temperature; WT, wild-type.

[1] To whom correspondence should be addressed (email hui.lu@manchester.ac.uk).

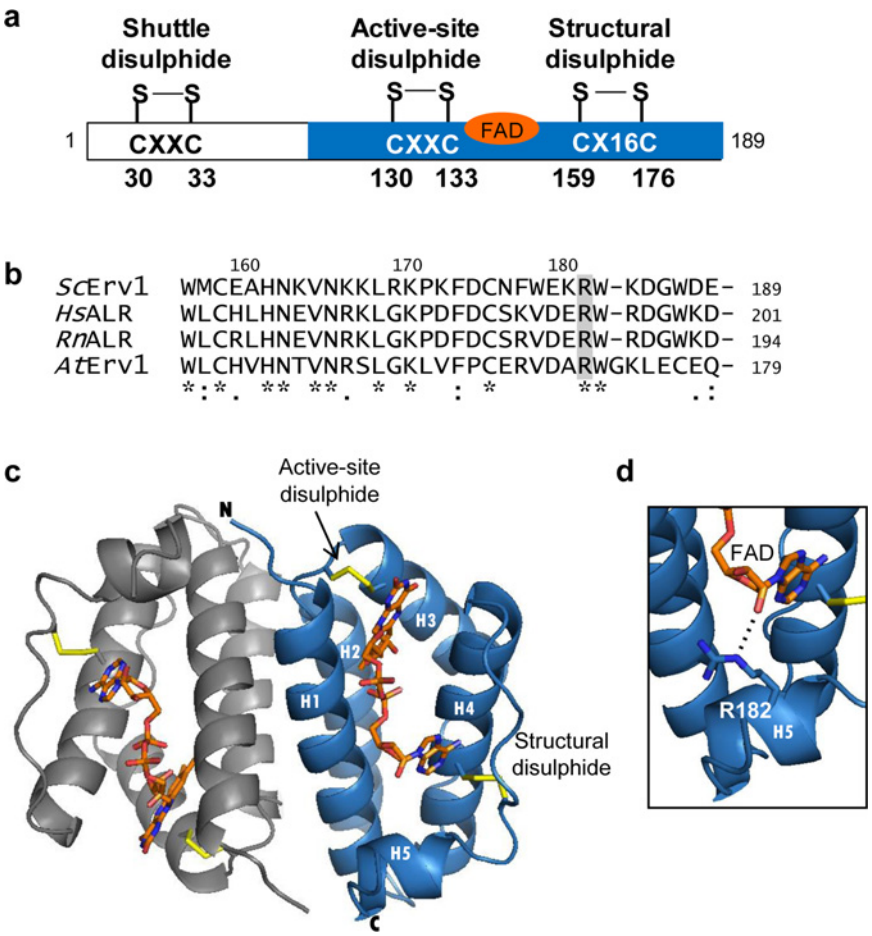


**Figure 1 Structure and sequence alignment of Erv/ALR proteins**

(**a**) Schematic of the primary structure of Erv1 with its three disulfide bonds and the conserved cysteine motifs. (**b**) Sequence alignment of the C-terminus of Erv/ALR proteins. The relevant arginine (R) residue is highlighted. *Sc*, *Sacharomyces cerevisiae*; *Hs*, *Homo sapiens*; *Rn*, *Rattus norvegicus*; *At*, *Arabidopsis thaliana*. (**c** and **d**) The X-ray crystal structure of yeast *S. cerevisiae* Erv1 core domain residues 84–188 (**c**) and a zoomed in of the structure showing the hydrogen bond formed between $Arg^{182}$ and the 2′OH of the ribose moiety of FAD (**d**) (PDB code: 4EOH [9]). The structures were generated using the PyMOL software.

susceptibility of the protein, but has only a minimal effect on its enzymatic activity [25]. A more recent study used yeast as a model to show that, at the restrictive temperature of 37 °C, the ALR R194H mutant affected the accumulation of human Mia40 (hMia40) and other substrate proteins of the MIA pathway in the mitochondrial IMS [26].

In the present study, the effects of the R182H mutation on the folding, stability and the function of yeast Erv1 were characterized using a combination of *in vitro* and *in vivo* assays. Similar to the case of $Arg^{194}$ in human ALR [25], the $\delta$-nitrogen of $Arg^{182}$ forms a hydrogen bond with the 2′OH of the ribose moiety of FAD (Figure 1d) and the residue is also nearly co-planar with $Trp^{183}$, suggestive of a cation–$\pi$ interaction. In the present study, we first show that the mutation does not affect the initial binding of the FAD cofactor by Erv1, but it does affect the secondary, tertiary and quaternary structure of the protein. Secondly, thermal denaturation studies showed that Erv1 R182H is less stable than Erv1 wild-type (WT), with the mutation causing a decrease of ~10 °C in the melting temperature ($T_m$) of Erv1. Thirdly, a clear and progressive functional defect in the enzymatic activity of Erv1 was observed for the R182H mutant at both 25 °C and 37 °C. This functional defect was recovered by addition of excess free FAD (fFAD) and became less obvious with the increase in the Erv1 concentration in the assays, suggesting impairment in cofactor-binding by the catalytic intermediates of Erv1 R182H. Finally, using yeast genetic methods, we verified our *in vitro* findings *in vivo*. Overall, the results of the present study provide significant insights into the effects of the R182H mutation on Erv1 and could potentially be extended to human ALR to better understand the molecular basis of autosomal recessive myopathy.

## EXPERIMENTAL

### Site-directed mutagenesis

A construct encoding the C-terminally $LE(H)_6$-tagged full-length WT Erv1 cloned into the expression vector pET-24a(+) (Novagen) was used as a DNA template to generate the Erv1 R182H mutant for protein purification. The primers 5′-TA-ATTTCTGGGAAAAACACTGGAAGGACGGCTGGGACGA-3′ and 5′-TCGTCCCAGCCGTCCTTCCAGTGTTTTTCCCAG-AAATTA-3′ were used for site-directed mutagenesis and the construct was verified by DNA sequencing.

### *In vivo* methods

A *S. cerevisiae* Δ*erv1* knockout strain containing R182H *ERV1* on a *TRP1* plasmid [24] was transformed with *URA3* plasmid pYES2 (Sigma–Aldrich) containing WT or R182H *ERV1* under the regulation of a *GAL10* promoter. Following selection, the transformants were plated on 5-fluoroanthranilic acid (FAA) solid medium to counter-select against TRP1-containing plasmid by incubating for up to 3 days at 30 °C. For overexpression of Erv1, selected individual colonies were grown on synthetic selective media with galactose (2 %) for 2 days at 30 °C before spot-testing on agar plates at 30 °C or 37 °C. Erv1 overexpression was analysed by Western blot of cellular extracts using Erv1 antibodies.

### Protein purification

The pET-24a(+) plasmid containing the WT or R182H *ERV1* gene was expressed in *Escherichia coli* Rosetta-gami™ 2 cells (Novagen). Cells were grown in 6 × 1 litres of LB medium at 37 °C until a $D_{600}$ of 0.3–0.4 was reached. Expression of the LE(H)$_6$-tagged Erv1 proteins was induced by addition of 0.5 mM IPTG (ForMedium) in the presence of 10 μM FAD (Sigma) for no longer than 16 h at 16 °C. Cells were centrifuged, resuspended in 6 × 20 ml of binding buffer (40 mM imidazole, 50 mM Tris/HCl and 150 mM NaCl, pH 7.4) and complemented again with 10 μM FAD. Cells were disrupted by sonication in the presence of three EDTA-free protease inhibitor cocktail tablets (Roche) and the cell lysate was centrifuged at 39 800 ***g*** for 60 min at 4 °C. The supernatant was added to a column with 5 ml of Ni-NTA ($Ni^{2+}$-nitrilotriacetate) His-Bind beads (Novagen) equilibrated with binding buffer. The column was washed with at least 5× bed volumes (BV) of binding buffer followed by 10× BV of washing buffer (80 mM imidazole, 50 mM Tris/HCl and 150 mM NaCl, pH 7.4). The bound LE(H)$_6$-tagged Erv1 proteins were eluted with 15–20 ml of elution buffer (500 mM imidazole, 50 mM Tris/HCl and 150 mM NaCl, pH 7.4) and an extra 100 μM of FAD were added. All column steps were performed at 4 °C. The proteins were divided into 500 μl aliquots, snap-frozen with liquid nitrogen and kept at −80 °C until use. Further purification was done by size-exclusion chromatography (SEC) using buffer AE (BAE: 50 mM Tris/HCl, 150 mM NaCl and 1 mM EDTA, pH 7.4) on a Superdex 200 100/300 GL column (GE Healthcare).

For purification of the GST–Mia40c (Mia40c: residues 284–403) the pGEX 4T-1 Vector (GE Healthcare) containing the *MIA40c* gene was expressed in *E. coli* BL21 (DE3) cells (Stratagene). Cells were grown in 12 × 1 litres of LB media at 37 °C until a $D_{600}$ of 0.3–0.4 was reached. Expression of the GST–Mia40c-tagged proteins was induced for 16–20 h at 16 °C by addition of IPTG to a final concentration of 0.5 mM. Cells were centrifuged and resuspended in a total of 200 ml of buffer A (BA: 50 mM Tris/HCl, 150 mM NaCl, pH 7.4). Cells were disrupted by sonication in the presence of six EDTA-free protease inhibitor cocktail tablets and the cell lysate was centrifuged at 39 800 ***g*** for 60 min at 4 °C. The supernatant was mixed with 20 ml of glutathione–Sepharose 4B beads (GE Healthcare) for 16–20 h at 4 °C. The column was washed with at least 15× BV of BA and then thrombin was added to a 10–15 units/ml final concentration. After incubation for 16 h at 4 °C, the cleaved protein was collected and the fractions containing Mia40c were pooled and concentrated. The purified protein includes an iron-bound proportion of Mia40c [27]. To remove the iron, the protein was treated to three dialysis steps (24 h each) in BA with diminishing EDTA concentrations (350 mM, 50 mM and 1 mM). Further purification was done using a 5 ml HiTrap Q HP ion-exchange column (GE Healthcare) and a 109–208 mM NaCl gradient. The protein was divided into 500 μl aliquots and kept at −20 °C until use. For preparation of rMia40c, the protein was incubated with 8 mM TCEP [tris(2-carboxyethyl)phosphine] for 1 h at 25 °C. Excess TCEP was then removed using a Superdex 75 100/300 GL column and an ÄKTApurifier system inside an anaerobic glove box (Belle Technology), with oxygen levels maintained below 2 p.p.m. Buffers were made anaerobic by extensive bubbling with oxygen-free nitrogen, prior to incubation inside the anaerobic glove box. The concentration of rMia40c was determined using an $\varepsilon_{280}$ of 11.7074 $mM^{-1}\cdot cm^{-1}$ as predicted using the ProtParam software.

To obtain oxidized cyt *c*, the partially oxidized protein (Sigma, ∼70 % oxidized) was dissolved in BAE and treated with 40 mM potassium ferricyanide for 1 h at 25 °C. Next, excess potassium ferricyanide was removed using a Superdex 75 column inside an anaerobic glove box, as described above. Only the peak representing the cyt *c* monomeric fraction was used for the experiments. Cyt *c* concentration was determined using the molar absorption coefficients of 8.4 $mM^{-1}\cdot cm^{-1}$ (oxidized) and 29.5 $mM^{-1}\cdot cm^{-1}$ (reduced) at 550 nm.

**Table 1 Summary of Erv1 WT and Erv1 R182H FAD-binding and stability**

Properties were determined at pH 7.4 unless otherwise stated. The parameters were determined under the same conditions for both proteins as described in the Experimental section. Results are means ± S.D., $n = 4$ (*) and $n = 2$ (†). MW, molecular mass.

| | Erv1 WT | Erv1 R182H |
|---|---|---|
| $\lambda_{max}$ (nm) | 460 | 459 |
| $\varepsilon$ ($mM^{-1}\cdot cm^{-1}$)* | 12.3 ± 0.1 | 11.8 ± 0.1 |
| % FAD* | 96 ± 6 | 93 ± 6 |
| MW (kDa)† | 90 ± 2 | 47 ± 3 |
| $T_m$ (°C, far-UV CD)* | 68 ± 5 | 60 ± 4 |
| $T_m$ (°C, near-UV CD)* | 69 ± 2 | 59 ± 2 |
| $T_m$ (°C, FAD fluorescence)* | 66 ± 2 | 57 ± 2 |
| $T_m$ (°C, FAD fluorescence, pH 7)† | 66 ± 2 | 57 ± 2 |
| $T_m$ (°C, FAD fluorescence, pH 6)† | 68 ± 3 | 59 ± 2 |
| $T_m$ (°C, FAD fluorescence, pH 5)† | 69 ± 2 | 60 ± 2 |

### Circular dichroism

CD analysis was done using a Chirascan CD spectrometer (Applied Photophysics) and either a 0.2 mm (far-UV) or a 5 mm (near-UV) pathlength quartz cuvette. Each spectrum represents an average of four independent scans (each scan repeated four times) with the spectra for buffer alone subtracted. Thermal denaturation was measured at 222 nm (far-UV) or 272 nm (near-UV) in 1 °C intervals over 10 °C–90 °C, with a temperature increase of 1 °C/min. The profiles represent the average for four independent experiments. $T_m$ values were calculated by obtaining the first derivative of each profile and finding the maximum.

### UV–visible spectroscopy

Absorption spectra were recorded from 250 to 700 nm, at 1 nm intervals, in a 1 cm pathlength quartz cuvette using a Cary 300 Bio UV-Vis spectrophotometer (Varian). Measurement of the molar absorption coefficient was done in BAE, as previously described [4,22]. The calculated molar absorption coefficients are summarized in Table 1.

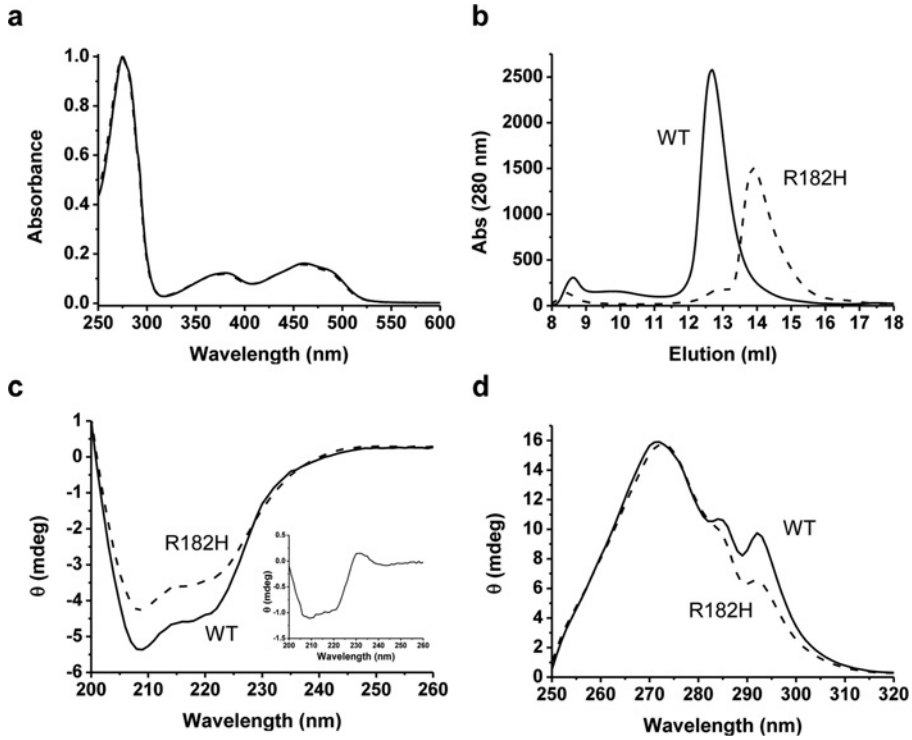


**Figure 2 Folding and oligomerization state of the WT and R182H mutant of Erv1**

(**a**–**d**) Erv1 WT (continuous line) and Erv1 R182H (broken line) (**a**) UV-visible spectra normalized at 275 nm. (**b**) Representative gel filtration chromatography profiles on a Superdex 200 column run in BAE. (**c**) Far-UV CD spectra of 0.22 mg/ml protein. Inset: subtraction of the R182H CD spectrum from that of the WT. The peak centred at ∼230 nm is characteristic of lost aromatic interactions. (**d**) Near-UV CD spectra of 0.5 mg/ml. All CD spectra represent the average of four independent measurements.

### Fluorescence spectroscopy

Fluorescence measurements were recorded using a Cary Eclipse fluorescence spectrophotometer (Varian) in a 1 cm × 0.2 cm path-length quartz cuvette. Thermal denaturation was followed by the increase in FAD fluorescence at 535 nm after excitation at 455 nm, in 1 °C intervals between 10 °C and 90 °C, with a temperature increase of 1 °C/min. Typically, the thermal denaturation and the FAD release profiles represent the average for four independent experiments.

For the experiments at different pH values, the buffers were as follows: 50 mM citrate, 150 mM NaCl and 1 mM EDTA, pH 5; 50 mM citrate, 150 mM NaCl and 1 mM EDTA, pH 6; 50 mM Hepes, 150 mM NaCl and 1 mM EDTA, pH 7.

### Oxygen consumption assay

Oxygen consumption was monitored using a Clark-type oxygen electrode (Hansatech Instruments). For measurements with TCEP as the substrate, the reactions were started by addition of 5 mM TCEP (pre-adjusted to pH ∼7) to an Erv1 solution in the presence of 80 units/ml of superoxide dismutase [28]. For reactions with rMia40c as the substrate, the reactions were started by addition of Erv1 to a solution of rMia40c. All reactions were done in BAE, unless otherwise stated, and the proteins were temperature equilibrated for 30 min to 2 h before the assays. For the experiments at different pH values, the buffers were as stated above. The Erv1 concentration in these assays is based on FAD content and was measured using the calculated FAD absorption coefficients in Table 1. Typically, each profile represents the average of 2–4 experimental measurements.

### Cytochrome *c* assay

A solution of Erv1/cyt *c* (syringe A) was mixed with rMia40c (syringe B) using a stopped flow instrument (Applied Photophysics) inside an anaerobic glove box, with oxygen levels maintained below 2 p.p.m. BAE was made anaerobic by extensive bubbling with oxygen-free nitrogen, prior to incubation inside the anaerobic glove box. Cyt *c* reduction was followed at 550 nm. For these experiments, Erv1 was buffer-exchanged into anaerobic BAE by SEC using a Superdex 200 column. The results represent the average for two independent experiments (four repeats in each experiment).

### FAD association and dissociation

For the association experiments, the apo-proteins of Erv1 WT and Erv1 R182H were prepared by treating the proteins with 8 M urea in BA while bound to a HisTrap HP column (GE Healthcare). Complete FAD release was monitored by the absorption at 280 nm. The apoproteins were then washed several times with BA prior to elution with 500 mM imidazole, 50 mM Tris/HCl and 150 mM NaCl, pH 7.4. Buffer exchange into BAE was done using a Superdex 200 column and the apo-Erv1 protein concentration was measured using an $\varepsilon_{280}$ of 42.315 $mM^{-1} \cdot cm^{-1}$ as predicted using the ProtParam software. Then, in the association experiments, the binding of equimolar amounts of FAD and apo-Erv1 was followed by the change in absorption at 496 nm using a stopped flow instrument at 25 °C. For the dissociation experiments, a freshly prepared 8 M urea solution (8 M urea, 50 mM Tris/HCl, 150 mM NaCl and 1 mM EDTA, pH 7.4) was mixed with Erv1 to give a final concentration of

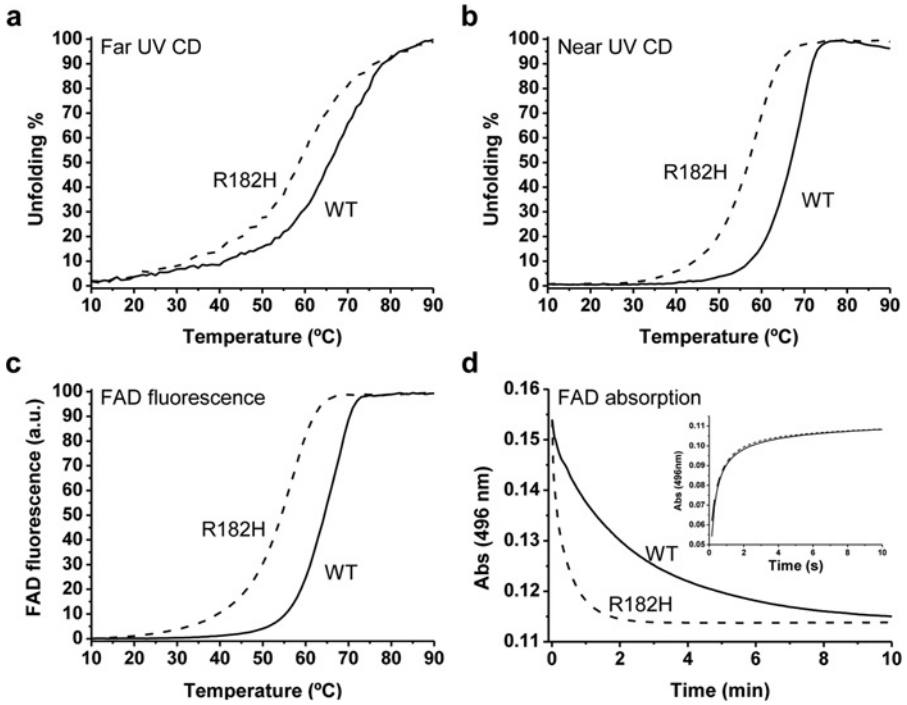


**Figure 3 Stability of the WT and R182H mutant of Erv1**

(**a**–**d**) Erv1 WT (continuous line) and Erv1 R182H (broken line). (**a**–**c**) Thermal denaturation followed by far-UV CD at 222 nm (**a**), near-UV CD at 272 nm (**b**) and FAD fluorescence (**c**) with excitation at 455 nm and emission at 535 nm. All profiles represent the average for four independent experiments. (**d**) Time course of FAD release from Erv1 by 7 M urea followed by absorbance at 496 nm. Half-lives of $1.8 \pm 0.2$ min and $0.3 \pm 0.1$ min (mean $\pm$ SD, $n = 3$) were determined for Erv1 WT and Erv1 R182H respectively. Inset: time courses of FAD binding to apo-Erv1 followed by the change in absorbance at 496 nm, the two curves are almost overlapping.

10 $\mu$M protein (based on FAD) and 7 M urea. The release of FAD at 25 °C was monitored by the change in absorption at 496 nm in a Cary 300 Bio UV-Vis spectrophotometer. All profiles represent the average for three experiments.

### Miscellaneous

Multiangle laser light scattering was done with purified protein applied to a Superdex 200 100/300 GL column running at a flow rate of 0.71 ml/min in BAE. Samples eluting from the column passed through an in-line DAWN HELEOS-II laser photometer ($\lambda = 658$ nm) and an Optilab rEX refractometer. Light scattering intensity and eluent refractive index (concentration) were analysed using ASTRA v5.3.4.13 software to give a weight-averaged molecular mass. The results represent the average for two independent experiments. The FAD-binding percentage of Erv1 was calculated by separately measuring the protein concentration using the BCA assay (according to the manufacturer's instructions) and the FAD concentration as stated above. The reported percentages represent an average of two independent measurements (four repeats in each measurement).

## RESULTS AND DISCUSSION

### Characterization of the effects of the R182H mutation on the folding and oligomerization state of Erv1

The Erv1 R182H mutant was expressed and purified from *E. coli* cells using the same method as for Erv1 WT (see the Experimental section). The R182H mutant exhibited the same yellowish colour as the WT and both proteins displayed the same overall UV–visible absorption spectra profiles (Figure 2a), suggesting that FAD-binding was not obviously affected by the mutation. Consistently, measurement of their FAD content showed that Erv1 WT and Erv1 R182H contained FAD at $96 \pm 6$ % and $93 \pm 6$ % respectively (Table 1).

On the other hand, gel filtration chromatography suggested that the mutant exists in a different oligomerization state (Figure 2b); although the WT eluted into a major peak at approximately 12.5 ml, the mutant eluted mainly at approximately 14 ml. The molecular masses of the fractions were then determined by multi-angle laser-light scattering to be $90 \pm 2$ kDa and $47 \pm 3$ kDa for WT and R182H respectively (Table 1). This indicates that the WT forms a tetramer and the R182H mutant forms a dimer (monomer Erv1 is 22.6 kDa). To date, Erv1 has been suggested to form oligomers with two or more subunits *in vitro* [16,29], with Erv1 adopting a dimer conformation being the current strongest interpretation [29]. In the present study, it appears that the R182H mutation disrupts the formation of Erv1 tetramer *in vitro*, but the importance of this finding remains unclear since the oligomerization state of Erv1 inside the cell is presently unknown.

Next, the conformation of both proteins was analysed using CD to gain more information on the folding of the mutant. The far-UV CD spectra of both the WT and the R182H mutant are representative of highly $\alpha$-helical proteins (Figure 2c), but the mutant displayed approximately 20 % lesser intensity than the WT, which indicates the mutant has a lower degree of secondary folding. Furthermore, subtraction of the R182H spectrum from that of the WT gave a positive peak centred at around 230 nm characteristic of strong aromatic–aromatic interactions [30]. Consistent with the present observation, different intensities in the near-UV CD tryptophan bands at 285 nm and 292 nm between WT and R182H were also observed (Figure 2d). Both these results suggest that the mutation probably disrupted some tertiary

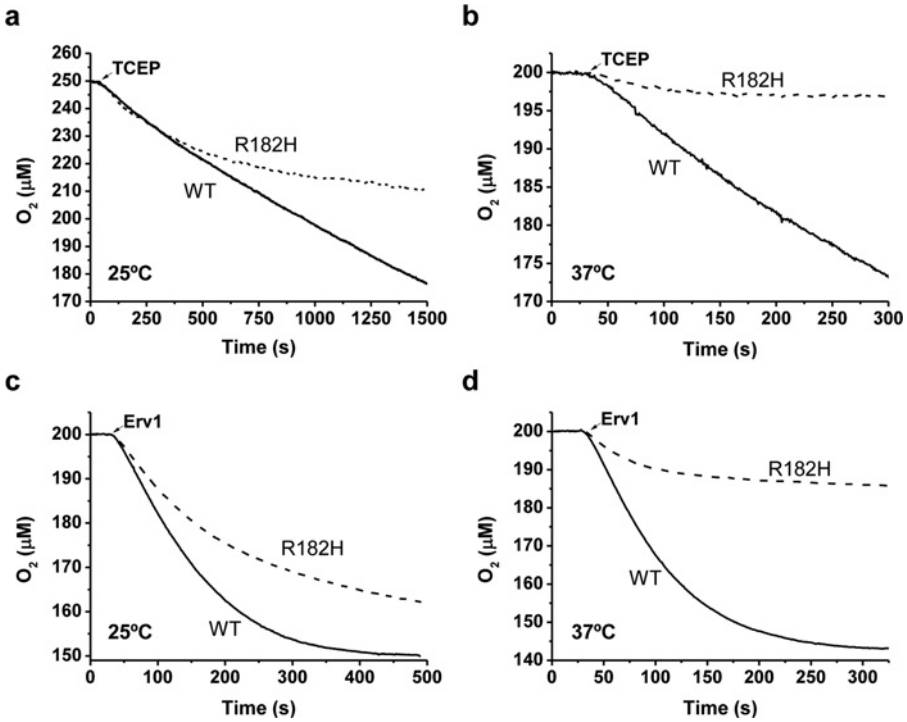


**Figure 4 Oxidase activity of the WT and R182H mutant of Erv1**

(**a** and **b**) Oxygen consumption profiles at 25 °C (**a**) and 37 °C (**b**) using 5 mM TCEP as the electron donor in the presence of 0.2 $\mu$M Erv1 WT (solid line) or Erv1 R182H (broken line) plus 80 units/ml of SOD (superoxide dismutase). (**c**) Oxygen consumption profiles of 0.2 $\mu$M Erv1 WT (continuous line) or Erv1 R182H (broken line) at 25 °C using 50 $\mu$M rMia40c as the electron donor. (**d**) As in (**c**) but at 37 °C and using 60 $\mu$M rMia40c. All profiles (TCEP and rMia40c) represent the average for two to four experiments.

tryptophan–aromatic interactions present in the Erv1 WT tetramer and that are lost in Erv1 R182H dimer. For example, the mutation may affect the interactions between $Trp^{183}$ (next to $Arg^{182}$) and other nearby aromatic residues (e.g. $Trp^{179}$) or, alternatively, it could affect the interaction between FAD and the aromatic residues that help in stabilizing it [6,9].

Taken together, these results showed that the R182H mutation does not affect the FAD content of Erv1, but does disturb its secondary, tertiary and quaternary structures.

### Influence of the R182H mutation on the stability of Erv1

Di Fonzo et al. [24] showed that the *erv1 R182H* yeast strain is temperature sensitive with a growth defect at 37 °C. Therefore, we studied the temperature-dependence of folding and FAD release using CD and FAD fluorescence. Similar thermal denaturation profiles were obtained using both far-UV CD at 222 nm and near-UV CD at 272 nm for Erv1 WT and Erv1 R182H (Figures 3a and 3b), which suggests that both proteins unfolded co-operatively in a two-state model. However, a difference of approximately 10 °C in their $T_m$ was observed (Table 1), indicating that R182H is less thermally stable than the WT. This ~10 °C decrease in $T_m$ is similar to the one obtained for ALR WT and its corresponding mutant ALR R194H [25]. Next, the temperature dependence of the relative FAD fluorescence intensity of both proteins (Figure 3c) was the same as the CD measurements, suggesting that the release of FAD from Erv1 was coupled with protein unfolding (Table 1). Despite the difference in $T_m$, at 37 °C there did not appear to be a drastic change in the folding of Erv1 and only approximately 5–10 % of FAD appeared to have been released from the mutant protein. Thus, it is difficult to conclude whether or not the lower thermal stability of Erv1 R182H is the main cause behind the defects caused by the mutant inside the cell.

Previous studies with ALR showed that the R194H mutant binds FAD more weakly than the WT, as displayed by its increased loss of FAD when treated with protein denaturants [25]. We, therefore, investigated whether the R182H mutation also affects the stability of FAD binding in Erv1. Figure 3(d) shows the time courses of FAD release upon addition of 7 M urea as measured by following the change in FAD absorption at 496 nm, the wavelength at which fFAD has a lower intensity than Erv1-bound FAD. Consistent with the results of ALR, the Erv1 R182H mutant lost its FAD more quickly than the WT protein and fitting of the profiles to an exponential decay gave half-lives of $1.8 \pm 0.2$ min for the WT and $0.3 \pm 0.1$ min for the R182H mutant. However, they both displayed the same FAD-binding kinetics (Figure 3d, inset), indicating that the off-rate ($k_{off}$) constant, but not the on-rate binding ($k_{on}$) constant, is affected by the mutation.

Histidine has a p$K_a$ of approximately 6, which means that under our experimental conditions (pH 7.4) histidine is expected to be largely deprotonated and uncharged. To understand the role of $His^{182}$ protonation (positive charge) on Erv1 stability, we repeated the FAD fluorescence thermal denaturation experiments at lower pH values (pH 5, 6 and 7), but no significant change in $T_m$ could be observed for both the WT and the R182H mutant (Table 1). Thus, it appears that protonation of $His^{182}$ is not important for the stability of the mutant.

In summary, the stability studies show that the R182H mutant has both decreased thermal stability and weaker FAD-binding compared with Erv1 WT. Similar destabilization effects were observed for ALR R194H [25], implying that the mutation has a direct and generalized effect on the stability of folding and cofactor-binding of Erv/ALR proteins.

### Effects of the R182H mutation on the activity of Erv1

We next investigated whether the structural and stability defects caused by the R182H mutation translated into a functional defect of Erv1. Initially, the oxidase activity of 0.2 $\mu$M Erv1 WT and Erv1 R182H was analysed using an oxygen consumption assay with TCEP as the electron donor at both 25 °C (Figure 4a) and 37 °C (Figure 4b). At 25 °C, although both proteins catalysed the reaction with similar rates initially ($0.07 \pm 0.01$ $\mu$M/s for WT and $0.08 \pm 0.01$ $\mu$M/s for R182H, $n = 4$), after approximately 300 s Erv1 R182H began to exhibit a progressive loss of activity. This functional defect was more drastic at 37 °C (Figure 4b) with the mutant becoming completely inactive almost from the start of the reaction.

To extend our finding to the physiological electron donor of Erv1, we repeated the oxygen consumption assays using 0.2 $\mu$M Erv1 and 50–60 $\mu$M rMia40c (Figures 4c and 4d). At 25 °C, Erv1 WT catalysed the reaction slightly faster than Erv1 R182H from the start of the reaction (Figure 4c), with initial rates ($v_0$) of $0.28 \pm 0.03$ $\mu$M/s and $0.20 \pm 0.01$ $\mu$M/s (n = 2) respectively. The progressive decay in the activity of the mutant was evident within a few seconds, but the protein still remained viable after 400 s. At 37 °C, the defect was again much stronger with the initial rate of the WT ($0.52 \pm 0.03$ $\mu$M/s, n = 2) being approximately 3-fold higher than that of the mutant ($0.16 \pm 0.01$ $\mu$M/s, $n = 2$) (Figure 4d) and the mutant becoming fully inactive after approximately 150 s. Changes of the redox state of rMia40c were then followed by AMS (4-acetamido-4′-maleimidylstilbene-2,2′-disulfonic acid) thiol-modification assay (Supplementary Figure S1) and the results were consistent with our oxygen consumption assays. Together these results indicate the R182H mutation caused a defect in the oxidase activity of Erv1 at 25 °C and that this defect is enhanced at 37 °C. Lastly, pre-incubation of Erv1 R182H at 37 °C followed by its return to 25 °C did not decrease its oxidase activity any further than expected (Supplementary Figure S2), which suggests that the harsher defect caused by the increase in temperature is reversible.

Inside the cell, both molecular oxygen and cyt *c* can act as electron acceptors of Erv1 [20–23]. Therefore we analysed the cyt *c* reductase activity of Erv1 inside an anaerobic glove box using rMia40c as the electron donor at 25 °C (Supplementary Figure S3) and 37 °C (Figure 5). A progressive decrease in the ability of Erv1 $Arg^{182}$ to reduce cyt *c* was clearly observed at 37 °C (Figure 5a). When the relative activity was calculated based on the initial rate, the R182H mutant displayed only $27 \pm 5$ % ($n = 8$) of the activity of the WT (Figure 5b). At 25 °C, the defect of the R182H mutant was also observed (Supplementary Figure S3), but to a lesser extent than at 37 °C. Overall, Erv1 R182H exhibited not only an apparent defect in its shuttling of electrons from TCEP/rMia40c to molecular oxygen but also in its cyt *c* reductase activity.

### Effects of the R182H mutation on the cofactor binding during the catalytic reaction

A possible explanation for the progressive inactivation of Erv1 R182H is that its weaker FAD binding is even more drastically decreased in one or more of the Erv1 catalytic intermediates, which could result in the loss of the cofactor (FAD or $FADH_2$) during catalytic turnover and cause Erv1 inactivation. To test this hypothesis, we recorded the absorption and fluorescence spectra of Erv1 in the FAD region with (+) and without (−) having catalysed the oxidation of rMia40c for 25 min at 37 °C (Figure 6). For Erv1 WT, the two absorption spectra (+ and −) are the same with an absorption maximum ($\lambda_{max}$) at 460 nm, characteristic of

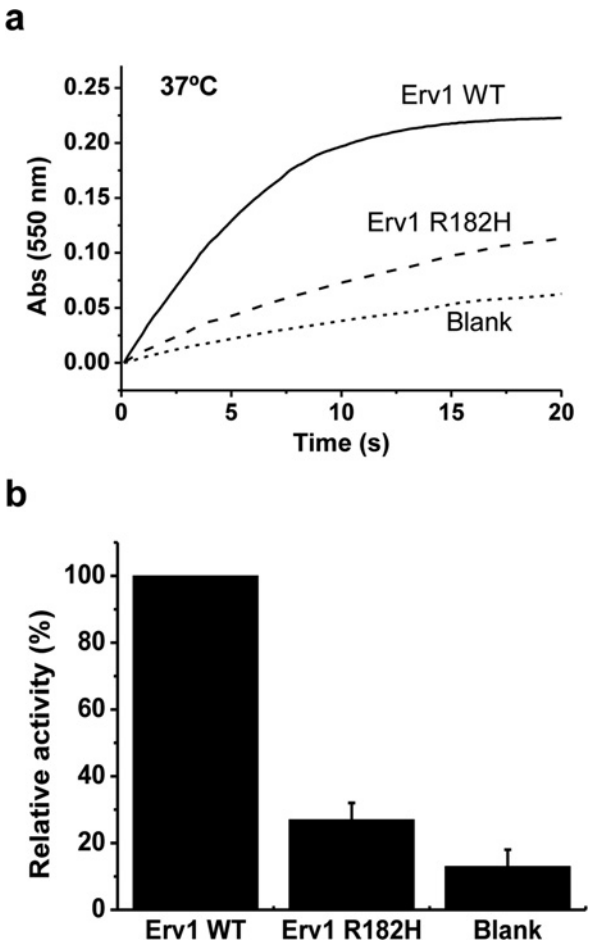


**Figure 5 Cyt *c* reduction catalysed by the WT and R182H mutant of Erv1 under anaerobic conditions**

(**a**) Representative time courses of cyt *c* reduction catalysed by 0.2 $\mu$M Erv1 and followed by the absorbance at 550 nm using anaerobic stopped-flow. Protein concentrations in the reaction: 30 $\mu$M rMia40c plus 40 $\mu$M cyt *c* in the absence (blank) or presence of 0.2 $\mu$M Erv1 WT (solid line) or Erv1 R182H (dash line). The experiments were carried out at 37 °C. (**b**) Relative initial rates of the cyt *c* reduction in (**a**), means ± S.D., $n = 8$.

Erv1-bound FAD (Figure 6a) [4,8,22]. In contrast, after incubation with rMia40c, the $\lambda_{max}$ of Erv1 R182H blue-shifted from its initial 459 nm to 450 nm, a $\lambda_{max}$ characteristic of fFAD (Figure 6b). These results indicate that, although the WT protein returned to its initial state after catalysing the redox reaction, Erv1 R182H did not. Instead, the FAD cofactor was apparently released from the R182H mutant upon incubation with rMia40c. The same conclusion was also drawn based on measurements of FAD fluorescence (Figures 6c and 6d). When excited at 455 nm, fFAD gives a fluorescence spectrum with an emission maximum at 525 nm, but FAD fluorescence is generally quenched when bound to Erv1. In the present study, although the FAD fluorescence of Erv1 WT remained unchanged regardless of whether rMia40c was added or not (Figure 6c), the FAD fluorescence of Erv1 R182H displayed a ∼2.5-fold increase in intensity when in the presence of rMia40c (Figure 6d), which suggests FAD was released into the solution. Time course measurements then confirmed that the release of FAD from Erv1 R182H only occurred upon addition of rMia40c, incubation of R182H alone at 37 °C for 25 min did not cause FAD to be released (Figure 6e).

To understand whether the release of the cofactor is caused by a specific interaction between Erv1 and rMia40c, the time-course

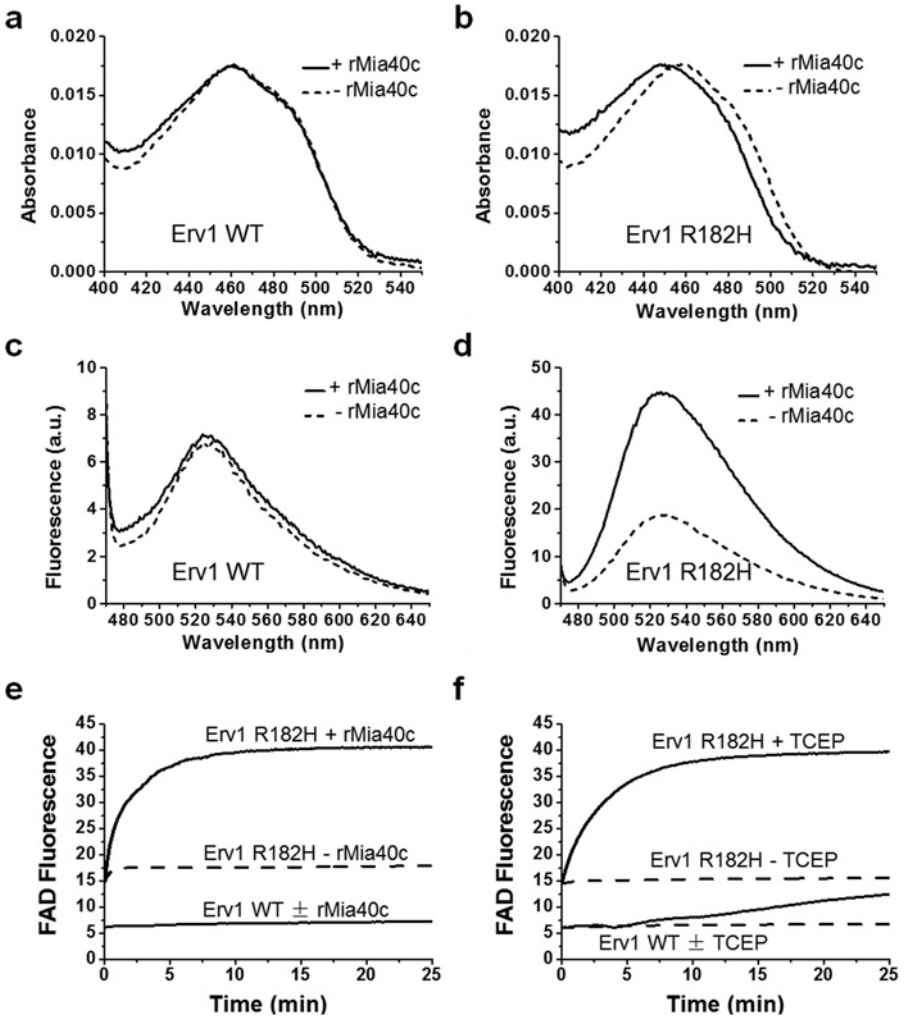


**Figure 6 Release of the cofactor during the catalytic reaction of Erv1**

Absorption spectra (**a** and **b**) and FAD fluorescence spectra (**c** and **d**) of 1.5 $\mu$M Erv1 WT (**a** and **c**) and Erv1 R182H (**b** and **d**) recorded after 25 min incubation in the presence (continuous lines) or absence (broken lines) of 140 $\mu$M rMia40c at 37 °C. (**e**). Time courses of FAD fluorescence intensity change during the oxidation of rMia40c in the absence and presence of Erv1 WT or Erv1 R182H. The reactions conditions were the same as in (**a**) to (**d**). (**f**) As in (**e**), but 5 mM TCEP was used instead. All time courses (TCEP and rMia40c) represent the average for four independent experiments.

FAD fluorescence experiments were repeated using the alternative electron donor TCEP (Figure 6f). In this case, a similar result was observed where TCEP also caused the cofactor release, indicating that the defect is not specific to rMia40c. The slight fluorescence intensity increase for the WT after approximately 6 min of TCEP addition is caused by the depletion of oxygen in the solution. Because the release of the cofactor from Erv1 R182H occurred only when in the presence of a reducing agent (rMia40c or TCEP), these results indicate the release must occur from either one or more of the Erv1 reaction intermediates (e.g. the S-FAD charge-transfer complex or $FADH_2$-Erv1) [16] present during its catalytic cycle.

### The functional defect of Erv1 R182H can be recovered by addition of FAD or increasing the Erv1 concentration

The results so far indicate the cofactor is detached from Erv1 R182H during its catalytic reaction, thereby inactivating the protein. Therefore we tested whether addition of extra FAD could recover the activity of the R182H mutant in an oxygen consumption assay, when using TCEP as the substrate. Interestingly, although 50 $\mu$M fFAD consumed oxygen slowly (Supplementary Figure S4) when in the presence of fFAD, the R182H mutant no longer became progressively inactive at 25 °C and behaved like the WT protein (Figure 7a). The oxidase activity of Erv1 R182H at 37 °C was also fully recovered in the presence of excess fFAD (Figure 7b), with initial rates of $0.11 \pm 0.01$ $\mu$M/s ($n = 2$) and $0.13 \pm 0.02$ $\mu$M/s ($n = 4$, Figure 4b) for R182H plus fFAD and WT respectively.

Previous reports regarding Erv1 R182H have suggested the mutation may specifically affect the transfer of electrons from rMia40c to Erv1 or from Erv1 to cyt *c* [24,26]. However, the results of the present study offer a different explanation to these functional defects. The fact that addition of fFAD recovered the enzymatic activity of the Erv1 R182H mutant indicates that the specific interactions between Erv1 and rMia40, molecular oxygen and cyt *c* are not directly affected. The defects observed are instead caused by an intrinsic inactivation of Erv1 itself, which would in turn appear to disrupt all its other interactions.

Interestingly, a way of apparently recovering the activity of the mutant consisted in increasing the Erv1 concentration in the

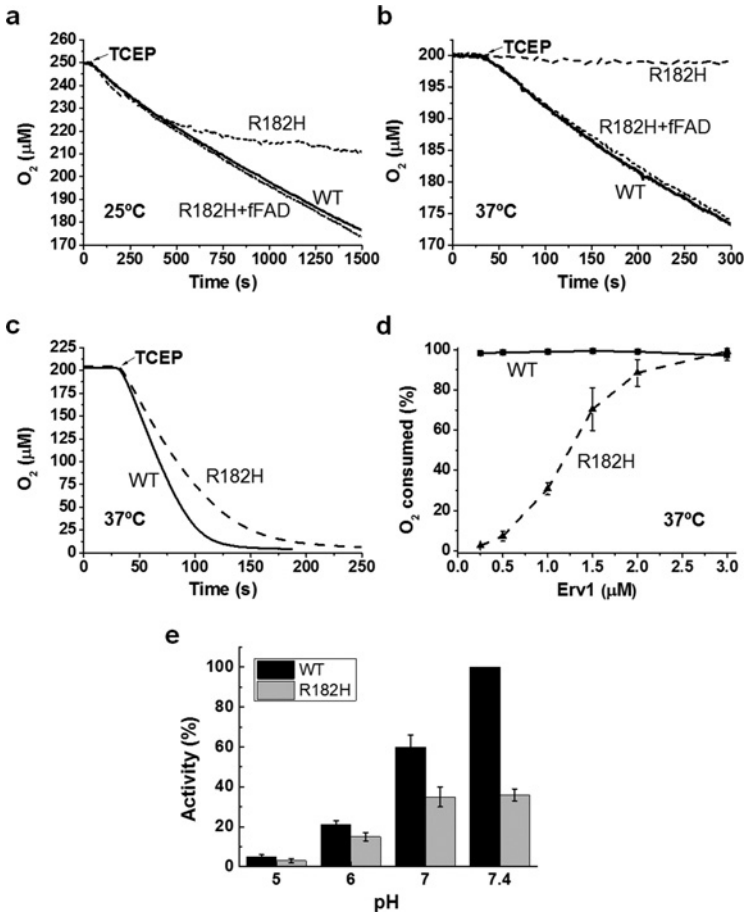


**Figure 7 Recovery of the enzymatic activity of the Erv1 R182H mutant**

(**a** and **b**) Oxygen consumption profiles of 0.2 $\mu$M Erv1 R182H in the presence (short dash line) or absence (dash line) of 50 $\mu$M fFAD. The reactions were carried out at either 25 °C (**a**) or 37 °C (**b**) using 5 mM TCEP as the electron donor in the presence of 80 units/ml SOD (superoxide dismutase). The profile of Erv1 WT (continuous line) was added for comparison. (**c**) Oxygen consumption profiles of 3 $\mu$M Erv1 WT (continuous line) and Erv1 R182H (broken line) at 37 °C using 5 mM TCEP as the electron donor in the presence of 80 units/ml SOD. (**d**) Erv1 concentration-dependence of the relative amount of oxygen consumed when using 5 mM TCEP as the electron donor at 37 °C in the presence of 80 units/ml SOD (means $\pm$ S.D., $n = 2$–4). (**e**) Change in the relative activity, based on the initial rate, of Erv1 WT and Erv1 R182H at different pH values when measured in an oxygen consumption assay at 37 °C (means $\pm$ S.D., $n = 3$). Reactions conditions: 1 $\mu$M Erv1, 5 mM TCEP and 80 units/ml SOD.

activity assays. Our above experiments (Figures 4–6, 7a and 7b) were done using an Erv1 concentration of 0.2 $\mu$M; however, when similar experiments were performed using 3 $\mu$M Erv1, the defect of the R182H mutant was less obvious (Figure 7c). Despite Erv1 R182H reacting at a lower rate ($v_0 = 2.2 \pm 0.2$ $\mu$M/s, $n = 4$) than that of Erv1 WT ($v_0 = 2.9 \pm 0.1$ $\mu$M/s, $n = 4$), the mutant was capable of consuming all of the oxygen in the chamber at 37 °C. The final amount of oxygen consumed by Erv1 R182H before it became fully inactive was in fact dependent on its initial concentration in the assay (Figure 7d). Furthermore, the initial rates of both proteins also increased with the Erv1 concentration in an almost parallel manner, but the R182H mutant was consistently less active than the WT (Supplementary Figure S5). A feasible interpretation of these results is that the mutant is initially active and remains so for a number of enzymatic turnovers, allowing it to consume a certain amount of oxygen. Increasing the initial concentration of Erv1, therefore, also increases the total amount of oxygen consumed, with the limit being the initial amount of oxygen in the chamber (200–250 $\mu$M). A previous study by Daithankar et al. [25] showed that the enzymatic activity of ALR was only minimally affected by the R194H mutation, with no report of its cofactor being lost during the catalytic reaction. The study was done by measuring the steady-state enzyme-kinetic parameters of ALR WT and ALR R194H at 25 °C, a temperature at which at least the defect of the Erv1 R182H mutant is not always detectable (Supplementary Figure S6). However, ALR is thermally more stable than Erv1, so it is possible the activity defect is more easily detectable for Erv1. It would be interesting to see if the same behaviour, where the defect is only evident under certain reaction conditions (e.g. low enzyme concentration, 37 °C), also occurs with ALR R194H.

To know whether histidine protonation plays a critical role in the functional defect of Erv1 R182H, we repeated the oxygen consumption assays at lower pH values using TCEP as the electron donor in the presence of 1 $\mu$M Erv1 (Supplementary Figure S7). Although the activity of both the WT and the R182H decreased with pH, the mutant still consistently showed a relative lower activity than the WT (Figure 7e). However, the observed defect appears to become relatively smaller as the pH decreases, implying that protonation of $His^{182}$ in the mutant protein does play a role in stabilizing the binding of the FAD cofactor during the reaction, but it is not the only reason behind the functional defect.

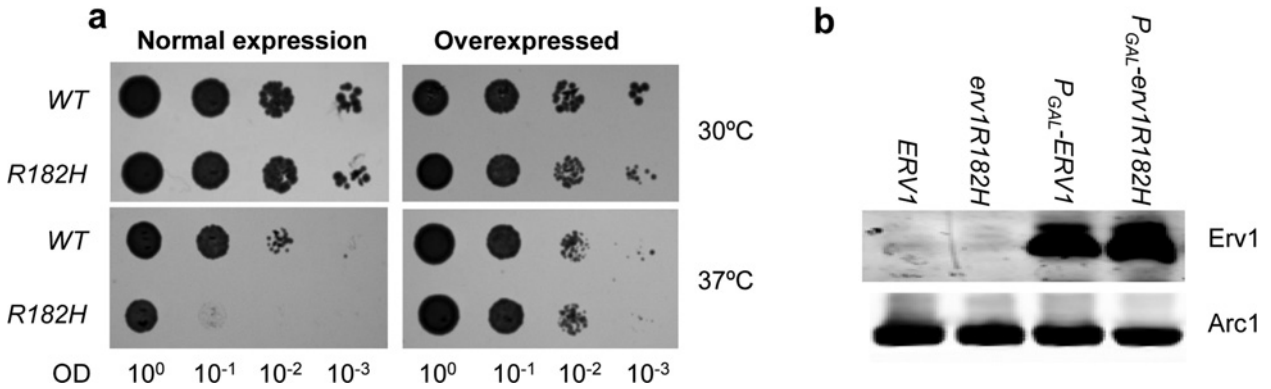


**Figure 8** ***In vivo*** **test of the overexpressed Erv1**

(**a**) Spot-test of *S. cerevisiae* yeast strains expressing Erv1 WT or Erv1 R182H. For expression of endogenous levels of Erv1, Δ*erv1* yeast strains carrying single copy plasmids expressing Erv1 WT or Erv1 R182H from the endogenous *ERV1* promoter were spotted on to the selective medium containing 2 % glucose. For overexpression, Δ*erv1* strains carrying multi-copy plasmids expressing Erv1 WT or Erv1 R182H from the *GAL10* promoter were grown in liquid medium containing 2 % galactose for 24 h and then spotted on to the selective medium containing 2 % galactose. (**b**) Western blot analysis of Erv1 levels from the strains used in (**a**). Arc1 served as a loading control.

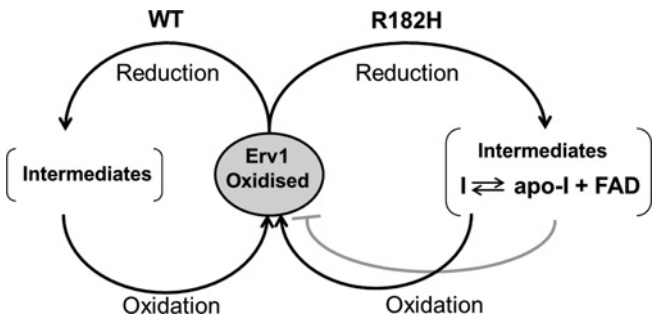


**Figure 9 Model for the functional defect of Erv1 R182H**

The oxidized form of both Erv1 WT and Erv1 R182H is stable under physiological conditions. Upon reduction by an electron donor (e.g. TCEP or rMia40c), Erv1 goes through a series of catalytic intermediates before returning to its initial oxidized state by reacting with molecular oxygen or cyt *c*. All molecules of the WT protein can be recycled back to the oxidized state, but a fraction of the R182H mutant loses its FAD cofactor from one or more of the catalytic intermediates during each redox cycle which results in a progressive loss of FAD and decreased activity.

### Testing the *in vitro* finding *in vivo*

On the basis of the results outlined above, we predicted that the growth defect of the *erv1 R182H* mutant yeast strain reported by Di Fonzo et al. [24] could be rescued by increasing the steady-state concentration of the mutant protein. Therefore, we overexpressed the WT and R182H mutant protein in the yeast *S. cerevisiae* and performed a spot-test of both strains at the permissive (30 °C) and non-permissive (37 °C) temperatures (Figure 8a). The results showed that the 37 °C growth defect was indeed rescued by the overexpression of Erv1 R182H with both the WT and the R182H mutant being overexpressed in similar amounts (Figure 8b).

### Conclusion

In the present report, we characterized and compared the WT and R182H mutant of yeast Erv1 using a combination of structural and functional methods. We provided clear evidence for an apparent defect in the catalytic activity of Erv1 caused by the R182H mutation, which allowed us to propose a model for the molecular mechanism of the disease. Our results show that despite the effects of the R182H mutation on the folding, thermal stability and FAD-binding of the fully oxidized state of Erv1, these are not sufficient to disrupt the catalytic activity of the protein. Instead, we showed that the cofactor was released from Erv1 R182H during its catalytic cycle, leading to a gradual inactivation of the protein (Figure 9). Previous studies have shown that Erv1 and ALR use similar catalytic mechanisms and go through several intermediate states (e.g. the S-FAD charge-transfer complex, $FADH_2$–Erv1) during their catalytic cycle [16,31–33], so it would be interesting to see if the ALR R194H mutant also loses its cofactor during its catalytic cycle. We cannot conclude at which stage of the catalytic cycle the cofactor is released and the R182H mutation may affect more than one Erv1 intermediate. Finally, our results also suggest that the interaction of Erv1 with rMia40c, oxygen and cyt *c* is not directly affected by the R182H mutation, but instead the observed defects are a side effect of the inactivation of Erv1 by its loss of FAD.

## AUTHOR CONTRIBUTION

Efrain Ceh-Pavia and Hui Lu designed the research; Efrain Ceh-Pavia, Swee Ang and Michael Spiller performed experiments; Efrain Ceh-Pavia, Swee Ang, Michael Spiller and Hui Lu analysed the data; Efrain Ceh-Pavia and Hui Lu wrote the paper and all authors provided feedback.

## ACKNOWLEDGEMENTS

We thank Marjorie Howard and Thomas Jowitt of the Faculty Biomolecular Analysis core facility for their technical help with the light scattering measurements, Derren Heyes for his technical help with the anaerobic stopped-flow, Nigel Scrutton for helpful discussion, Stephen High for reading and providing helpful comments on the manuscript and Tiziana Lodi for the *erv1* deletion yeast strain.

## FUNDING

This work was supported by the Biotechnology and Biological Sciences Research Council [grant number BB/H017208]; the Leverhulme Trust [grant number F/00120/CB]; and a Ph.D. studentship from the Mexican National Council for Science and Technology (CONACyT) (to E.C.P.).

## REFERENCES

1 Chacinska, A., Koehler, C. M., Milenkovic, D., Lithgow, T. and Pfanner, N. (2009) Importing mitochondrial proteins: machineries and mechanisms. Cell **138**, 628–644 CrossRef PubMed

2 Fraga, H. and Ventura, S. (2013) Oxidative folding in the mitochondrial intermembrane space in human health and disease. Int. J. Mol. Sci. **14**, 2916–2927 CrossRef PubMed

3 Herrmann, J. M. and Riemer, J. (2012) Mitochondrial disulfide relay: redox-regulated protein import into the intermembrane space. J. Biol. Chem. **287**, 4426–4433 CrossRef PubMed

4 Ang, S. K. and Lu, H. (2009) Deciphering structural and functional roles of individual disulfide bonds of the mitochondrial sulfhydryl oxidase Erv1p. J. Biol. Chem. **284**, 28754–28761 CrossRef PubMed

5 Gross, E., Sevier, C. S., Vala, A., Kaiser, C. A. and Fass, D. (2002) A new FAD-binding fold and intersubunit disulfide shuttle in the thiol oxidase Erv2p. Nat. Struct. Biol. **9**, 61–67 CrossRef PubMed

6 Fass, D. (2008) The Erv family of sulfhydryl oxidases. Biochim. Biophys. Acta **1783**, 557–566 CrossRef PubMed

7 Hofhaus, G., Lee, J. E., Tews, I., Rosenberg, B. and Lisowsky, T. (2003) The N-terminal cysteine pair of yeast sulfhydryl oxidase Erv1p is essential for *in vivo* activity and interacts with the primary redox centre. Eur. J. Biochem. **270**, 1528–1535 CrossRef PubMed

8 Lee, J., Hofhaus, G. and Lisowsky, T. (2000) Erv1p from *Saccharomyces cerevisiae* is a FAD-linked sulfhydryl oxidase. FEBS Lett. **477**, 62–66 CrossRef PubMed

9 Guo, P. C., Ma, J. D., Jiang, Y. L., Wang, S. J., Bao, Z. Z., Yu, X. J., Chen, Y. and Zhou, C. Z. (2012) Structure of yeast sulfhydryl oxidase erv1 reveals electron transfer of the disulfide relay system in the mitochondrial intermembrane space. J. Biol. Chem. **287**, 34961–34969 CrossRef PubMed

10 Ceh-Pavia, E., Spiller, M. P. and Lu, H. (2013) Folding and biogenesis of mitochondrial small Tim proteins. Int. J. Mol. Sci. **14**, 16685–16705 CrossRef PubMed

11 Lu, H., Allen, S., Wardleworth, L., Savory, P. and Tokatlidis, K. (2004) Functional TIM10 chaperone assembly is redox-regulated *in vivo*. J. Biol. Chem. **279**, 18952–18958 CrossRef PubMed

12 Mesecke, N., Terziyska, N., Kozany, C., Baumann, F., Neupert, W., Hell, K. and Herrmann, J. M. (2005) A disulfide relay system in the intermembrane space of mitochondria that mediates protein import. Cell **121**, 1059–1069 CrossRef PubMed

13 Morgan, B. and Lu, H. (2008) Oxidative folding competes with mitochondrial import of the small Tim proteins. Biochem. J. **411**, 115–122 CrossRef PubMed

14 Milenkovic, D., Gabriel, K., Guiard, B., Schulze-Specking, A., Pfanner, N. and Chacinska, A. (2007) Biogenesis of the essential Tim9-Tim10 chaperone complex of mitochondria: site-specific recognition of cysteine residues by the intermembrane space receptor Mia40. J. Biol. Chem. **282**, 22472–22480 CrossRef PubMed

15 Sideris, D. P., Petrakis, N., Katrakili, N., Mikropoulou, D., Gallo, A., Ciofi-Baffoni, S., Banci, L., Bertini, I. and Tokatlidis, K. (2009) A novel intermembrane space-targeting signal docks cysteines onto Mia40 during mitochondrial oxidative folding. J. Cell Biol. **187**, 1007–1022 CrossRef PubMed

16 Ang, S. K., Zhang, M., Lodi, T. and Lu, H. (2014) Mitochondrial thiol oxidase Erv1: both shuttle cysteine residues are required for its function with distinct roles. Biochem. J. **460**, 199–210 CrossRef PubMed

17 Lionaki, E., Aivaliotis, M., Pozidis, C. and Tokatlidis, K. (2010) The N-terminal shuttle domain of Erv1 determines the affinity for Mia40 and mediates electron transfer to the catalytic Erv1 core in yeast mitochondria. Antioxid. Redox Signal. **13**, 1327–1339 CrossRef PubMed

18 Rissler, M., Wiedemann, N., Pfannschmidt, S., Gabriel, K., Guiard, B., Pfanner, N. and Chacinska, A. (2005) The essential mitochondrial protein Erv1 cooperates with Mia40 in biogenesis of intermembrane space proteins. J. Mol. Biol. **353**, 485–492 CrossRef PubMed

19 Tienson, H. L., Dabir, D. V., Neal, S. E., Loo, R., Hasson, S. A., Boontheung, P., Kim, S. K., Loo, J. A. and Koehler, C. M. (2009) Reconstitution of the mia40-erv1 oxidative folding pathway for the small tim proteins. Mol. Biol. Cell. **20**, 3481–3490 CrossRef PubMed

20 Allen, S., Balabanidou, V., Sideris, D. P., Lisowsky, T. and Tokatlidis, K. (2005) Erv1 mediates the Mia40-dependent protein import pathway and provides a functional link to the respiratory chain by shuttling electrons to cytochrome *c*. J. Mol. Biol. **353**, 937–944 CrossRef PubMed

21 Bihlmaier, K., Mesecke, N., Terziyska, N., Bien, M., Hell, K. and Herrmann, J. M. (2007) The disulfide relay system of mitochondria is connected to the respiratory chain. J. Cell Biol. **179**, 389–395 CrossRef PubMed

22 Dabir, D. V., Leverich, E. P., Kim, S. K., Tsai, F. D., Hirasawa, M., Knaff, D. B. and Koehler, C. M. (2007) A role for cytochrome *c* and cytochrome *c* peroxidase in electron shuttling from Erv1. EMBO J. **26**, 4801–4811 CrossRef PubMed

23 Farrell, S. R. and Thorpe, C. (2005) Augmenter of liver regeneration: a flavin-dependent sulfhydryl oxidase with cytochrome *c* reductase activity. Biochemistry **44**, 1532–1541 CrossRef PubMed

24 Di Fonzo, A., Ronchi, D., Lodi, T., Fassone, E., Tigano, M., Lamperti, C., Corti, S., Bordoni, A., Fortunato, F., Nizzardo, M. et al. (2009) The mitochondrial disulfide relay system protein GFER is mutated in autosomal-recessive myopathy with cataract and combined respiratory-chain deficiency. Am. J. Hum. Genet. **84**, 594–604 CrossRef PubMed

25 Daithankar, V. N., Schaefer, S. A., Dong, M., Bahnson, B. J. and Thorpe, C. (2010) Structure of the human sulfhydryl oxidase augmenter of liver regeneration and characterization of a human mutation causing an autosomal recessive myopathy. Biochemistry **49**, 6737–6745 CrossRef PubMed

26 Sztolsztener, M. E., Brewinska, A., Guiard, B. and Chacinska, A. (2013) Disulfide bond formation: sulfhydryl oxidase ALR controls mitochondrial biogenesis of human MIA40. Traffic **14**, 309–320 CrossRef PubMed

27 Spiller, M. P., Ang, S. K., Ceh-Pavia, E., Fisher, K., Wang, Q., Rigby, S. E. and Lu, H. (2013) Identification and characterization of mitochondrial Mia40 as an iron-sulfur protein. Biochem. J. **455**, 27–35 CrossRef PubMed

28 Daithankar, V. N., Wang, W., Trujillo, J. R. and Thorpe, C. (2012) Flavin-linked Erv-family sulfhydryl oxidases release superoxide anion during catalytic turnover. Biochemistry **51**, 265–272 CrossRef PubMed

29 Bien, M., Longen, S., Wagener, N., Chwalla, I., Herrmann, J. M. and Riemer, J. (2010) Mitochondrial disulfide bond formation is driven by intersubunit electron transfer in Erv1 and proofread by glutathione. Mol. Cell **37**, 516–528 CrossRef PubMed

30 Martin, S. R. and Schilstra, M. J. (2008) Circular dichroism and its application to the study of biomolecules. Methods Cell Biol. **84**, 263–293 CrossRef PubMed

31 Banci, L., Bertini, I., Calderone, V., Cefaro, C., Ciofi-Baffoni, S., Gallo, A. and Tokatlidis, K. (2012) An electron-transfer path through an extended disulfide relay system: the case of the redox protein ALR. J. Am. Chem. Soc. **134**, 1442–1445 CrossRef PubMed

32 Kodali, V. K. and Thorpe, C. (2010) Oxidative protein folding and the quiescin-sulfhydryl oxidase family of flavoproteins. Antioxid. Redox Signal. **13**, 1217–1230 CrossRef PubMed

33 Schaefer-Ramadan, S., Gannon, S. A. and Thorpe, C. (2013) Human augmenter of liver regeneration: probing the catalytic mechanism of a flavin-dependent sulfhydryl oxidase. Biochemistry **52**, 8323–8332 CrossRef PubMed


Received 30 May 2014/15 September 2014; accepted 1 October 2014
Published as BJ Immediate Publication 1 October 2014, doi:10.1042/BJ20140679